Selective, direct detection of acetylcholine in PBS solution, with self-assembled fluorescent nano-particles: experiment and modelling
SUPPLEMENTARY MATERIAL

Lisa Peyrard[a], Claire Coiffier[b], Patrice Bordat[b], Didier Bégué[b], Sabine Chierici[c], Sandra Pinet[a], Isabelle Gosse[a,*], Isabelle Baraille[b], Ross Brown[b]

[a]*Institut des Sciences Moléculaires, umr 5255 du C.N.R.S., Institut Polytechnique de Bordeaux et Université de Bordeaux, 351, Cours de la Libération, 33405 Talence Cedex, France*
[b]*Institut des Sciences Analytiques et de Physico-Chimie pour l'Environnement et les Matériaux, umr 5254 du C.N.R.S., Université de Pau et des Pays de l'Adour, Hélioparc, 2 Av. du Pt. P. Angot, 64053 Pau Cedex 9, France*
[c]*Département de Chimie Moléculaire, umr 5250 du C.N.R.S., Université Joseph Fourier, Grenoble 1, B.P. 53, 38041 Grenoble Cedex 9, France*

Contents

*Corresponding author: gosse@enscbp.fr

1. Chemical and physical characterisation of compounds synthesized

Silica gel column chromatography purifications were performed on Scharlau 60 silica (40–60 μm) or Fluka Analytical 60 (40–63μm). Thin layer chromatography was done on silica layers (Merck, 60W F254S, 60 Å). NMR spectra of ^{1}H and ^{13}C were recorded at 400 MHz and 100 MHz on a Bruker Ultrashield Avance 400 spectrometer. Chemical shifts are reported using tetramethylsilane or the residual solvent peak as an internal reference for ^{1}H or for ^{13}C. Proton NMR spectral splitting patterns are reported below as: singlet (s), doublet (d) and broad signal (br). Infrared spectra were recorded in the range 4000-1000 cm^{-1}, on a Nicolet iS10 FT-IR spectrometer. Melting points were measured using Kofler Heizbank melting point benches (Reichert, model 7841, 150 W, or model WME, 100 W). Mass spectra were recorded at the CESAMO facility (Bordeaux, France) on a QStar Elite mass spectrometer (Applied Biosystems). The instrument is equipped with an ESI source and spectra were recorded in positive and negative ion mode. The electro-spray needle was maintained at 5000 V and operated at room temperature. Samples were dissolved in 50:50 DMSO/H_2O (99 % purity). The carrier solution was prepared by dissolving 10 mg of α-cyano-4-hydroxycinnamic acid (purity > 98.5 %) in 1 ml of 50:50 CH_3CN/H_2O 0.1 % TFA. Solutions were prepared at a 10:1 volume ratio of matrix to sample. One to two μl of solution were deposited on the sample target and dried under vacuum.

Characterisation of **3**

See fig. 1 for the NMR spectra. ^{1}H NMR,(400 MHz, $CDCl_3$) (δ, ppm): 8.01 (d, J = 8.6 Hz, 6H, Ar-H), 7.59 (d, J = 8.6 Hz, 6H, Ar-H), 7.49 (s, 3H, Ar-H), 6.91 (s, 3H, Ar-H), 4.78 (d, J = 13.6 Hz, 3H, Ar-CH_2), 3.94 (s, 9H, OCH_3), 3.93 (s, 9H, $COOCH_3$), 3.69 (d, J = 13.6 Hz, 3H, Ar-CH_2); ^{13}C NMR (100 MHZ, $CDCl_3$) (δ,ppm): 166.6 (COOMe), 159.1 (C_{Ar}), 141.9 (C_{Ar}), 134.9 (C_{Ar}), 131.5 (C_{Ar}), 130.8 (CAr), 129.4 (CAr), 129.3 (CAr), 128.4 (CAr), 112.5 (C_{Ar}), 111.0 (C_{Ar}), 92.4 (C≡C), 88.7 (C≡C), 56.3 (OCH_3), 52.2 ($COOCH_3$), 36.7 (Ar-CH_2);

IR (neat, ν, cm^{-1}): 3001, 2954, 2844, 2822, 2205, 1713, 1598, 1491, 1431, 1392, 1270, 1245, 1163, 1102, 1074; Melting point: 256 ° C; HRMS (ESI TOF/+MS) calcd. for $C_{54}H_{42}O_9$, Na adduct: calculated 857.2721, found 857.2729.

Characterisation of **1a**

See fig. 2 for NMR spectra. ^{1}H NMR (400 MHz, DMSO-D_6) (δ, ppm): 13.1 (br, 3H, COOH), 7.97 (d, J = 8 Hz, 6H, Ar-H), 7.80 (s, 3H, Ar-H), 7.61 (d, J = 8 Hz, 6H, Ar-H), 7.32 (s, 3H, Ar-H), 4.85 (d, J = 13.6 Hz, 3H, Ar-CH_2), 3.88 (s, 9H, OCH 3), 3.76 (d, J = 13.6 Hz, 3H, Ar-CH_2); ^{13}C NMR (100 MHZ, DMSO-D_6) (δ, ppm): 166.7 (COOH), 158.5 (C_{Ar}), 143.0 (C_{Ar}), 134.8 (C_{Ar}), 131.4 (C_{Ar}), 131.3 (C_{Ar}), 130.2 (C_{Ar}), 129.5 (C_{Ar}), 127.1 (C_{Ar}), 112.9 (C_{Ar}), 109.3 (C_{Ar}), 91.8 (C≡C), 89.1 (C≡C), 56.2 (OCH_3), 35.1 (Ar-CH_2); IR (neat, ν, cm^{-1}): 2929, 2851, 2822, 2654, 2208, 1688, 1598, 1556, 1491, 1406, 1388, 1271, 1245, 1163, 1070; Mp: decomposition from 255 ° C; HRMS (ESI TOF / -MS) m/z for $C_{51}H_{35}O_9$: calculated 791.2286, found 791.2309.

Dynamic light scattering measurements

The size of the nanoparticles was determined at 25 ° C, with a Zetasizer Nano ZS (Malvern instrument) with a HeNe laser, detection angle of $\theta_{diff} = 173°$. A 5×10^{-4} M solution of **1b** in PBS buffer was used.

Fluorescence measurements

Fluorescence spectra were recorded on a CARY Eclipse spectrophotometer at 25 ° C . Fluorescence quantum yields were measured by standard methods on air-equilibrated samples at room temperature, using quinine bisulphate in 0.5 M H_2SO_4 as reference ($\Phi_{ref} = 0.546$)[1]. The reported fluorescence quantum yields are within ±10 %. Fluorescence lifetimes were measured by time correlated single-photon counting (TCSPC) on an Edinburgh Instruments fluorimeter (FLS 920), at 25 ° C. Excitation was with a hydrogen-filled nanosecond flashlamp (repetition rate 40 KHz). The instrument response (FWHM *ca.* 1 ns) was determined by measuring the light scattered by a ludox suspension. The TCSPC

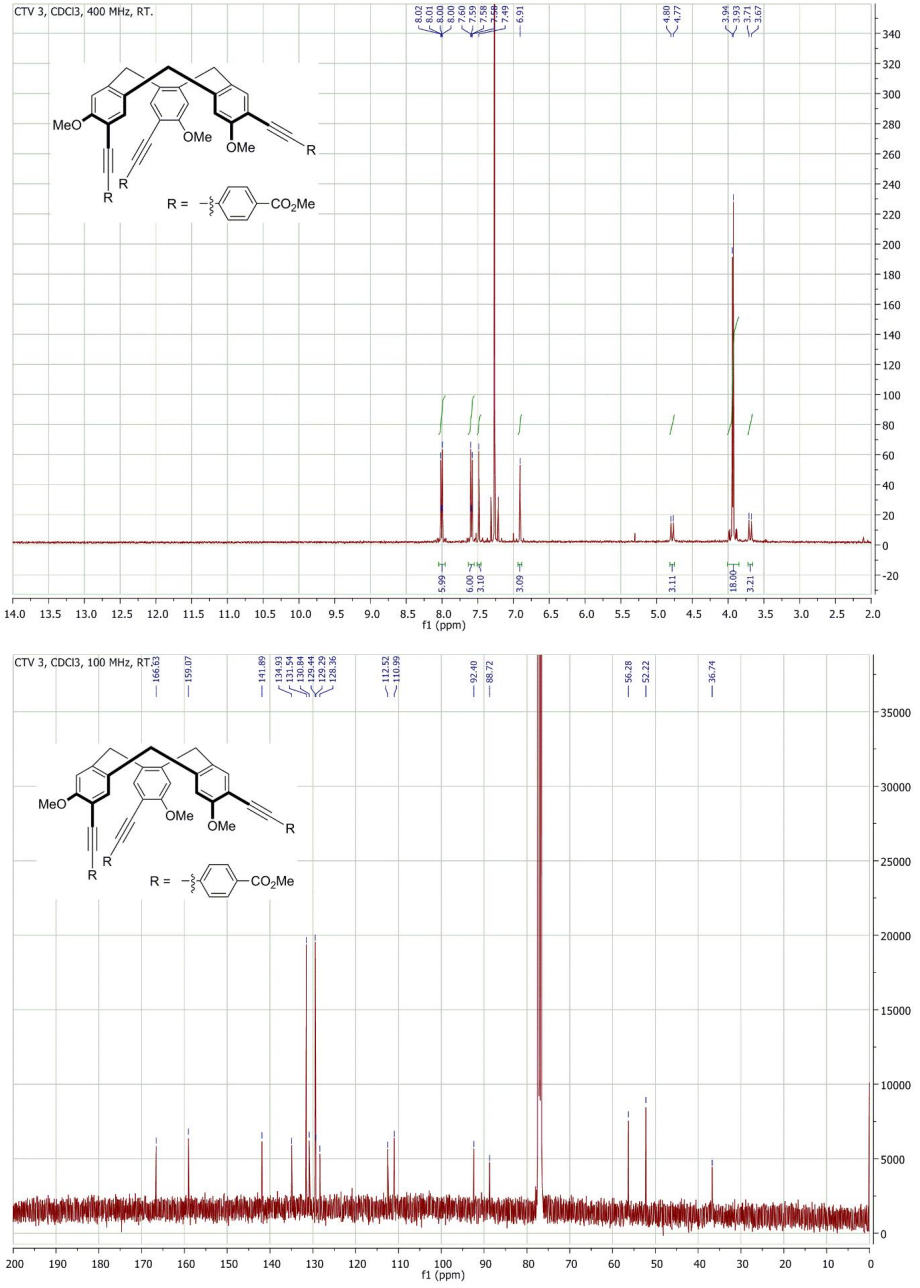

Figure 1: ^{1}H and ^{13}C NMR of CTV **3** in $CDCl_3$ at 298 K.

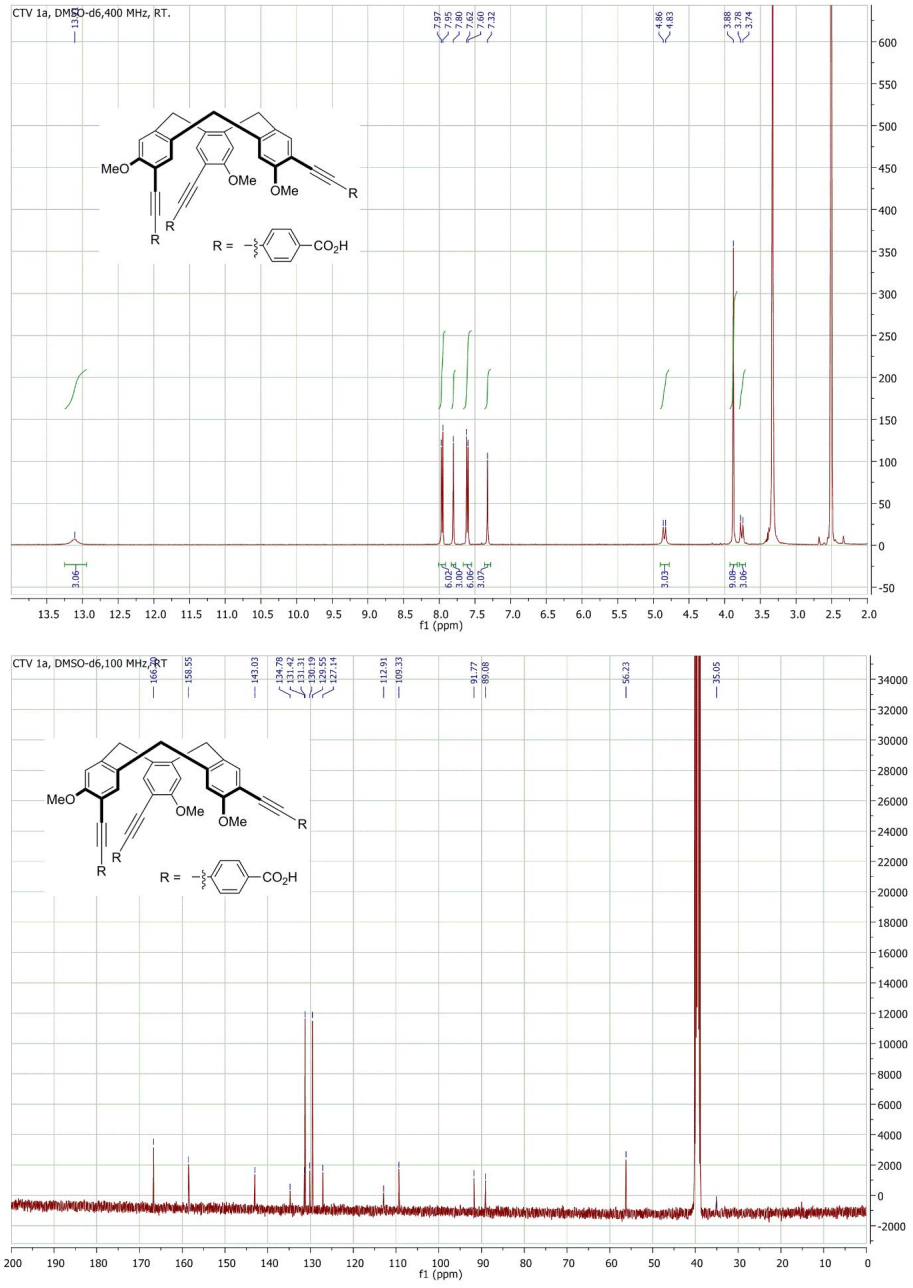

Figure 2: ^{1}H and ^{13}C NMR of CTV **1a** in DMSO-D_6 at 298 K .

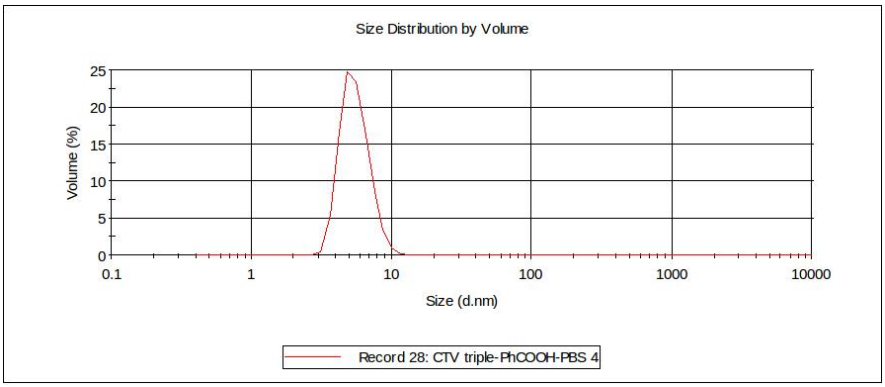

Figure 3: Dynamic light scattering spectrum of a solution of CTV **1b** at 10^{-4} M in PBS.

traces were analyzed by standard iterative reconvolution methods implemented in the software of the fluorimeter.

Transmission electron microscopy

The structure of the assembly formed from CTV **1a** was visualized by TEM. One drop of a 10^{-4} M solution of **1b** in PBS buffer was deposited on a copper grid coated with a layer of Formvar polymer, covered with a carbon membrane. The grid was observed with a Hitachi H7650 (120 kV) instrument using high resolution mode.

2. Simulations

Ab initio*,* DFT *and* TDDFT *calculations*

Before calculations on molecule **1a**, we examined a similar but smaller compound in order to choose computational methods: 2,3,7,8,12,13-hexamethoxy-10,15-dihydro-5H-tribenzo-[a,d,g]cyclononene[2], see SM fig. 5, referred to here as **4**. It has two methoxy- groups attached to each bowl ring, instead of one methoxy- and one (4-carboxyphenyl)ethynyl group as in **1a**, **1b**.

We compared density functionals with (ωB97XD) and without (B3LYP) long-range electron correlation, and two all electron basis sets, 6-31G and 6-311++G, augmented with standard polarisation and diffuse orbitals.

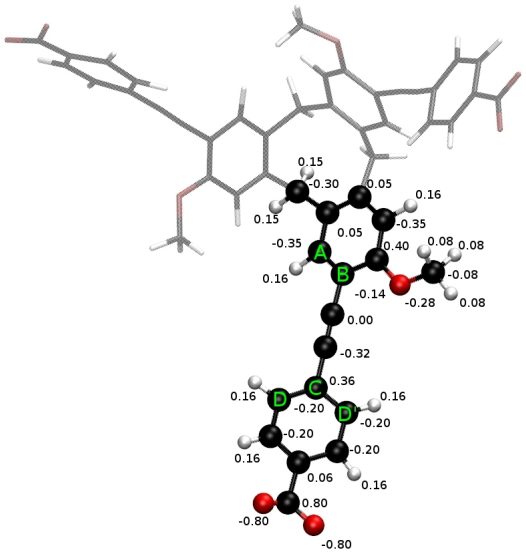

Figure 4: One arm of **1b**, showing, deviations from the OPLS-AA force field. Effective atomic point charges (shown in the figure) were derived from an electrostatic potential fit to the ωB97XD/6-311G(d,p) calculation. An additional torsional potential, $U(\phi) = A\,[1 + \cos(m\phi - \delta)]$, was applied to all quadruplets equivalent to A-B-C-D, A-B-C-D' with parameters $A = 0.0747\,\mathrm{kcal/mol}$, $m = 2$ and $\delta = 180\,^\circ$.

The crystal structure of **4** is known[3], but debatable as a reference. There are two pairs of molecules in the unit cell, the geometrical differences between them being bigger than between the theoretical methods and one of them, or between theoretical methods, see SM, fig. 2. Molecules in the crystal furthermore have a unique mirror plane, where three are expected from the topology, related by a C_3 axis. Packing a motif with a threefold axis into a monoclinic unit cell may be the cause of these discrepancies. Therefore we also ran MP2/6-31G(d,p) calculations as a further check. Table 1 in the supplementary information compares the results. Compared to X-ray diffraction (XRD) data, all the methods are good, with a slight advantage to ωB97XD compared to B3LYP, for bond lengths.

Molecular dynamics simulations

We performed classical molecular dynamics simulations on clusters of **1b** or the complex with ACh or Ch in vacuum and in water. The models of **1b** and the ammoniums were based on the OPLS-AA force field[4]. While the OPLS-AA partial charges correlate well with those from an electrostatic potential fit in the DFT computation (ωB97XD/6-3111++G(d,p), we prefer the latter, see fig. 4). The only other deviation from OPLS-AA is introduction of C-C≡C-C torsional potentials about the triple bonds in **1a**, **1b**, derived from a fit to DFT data, fig. 4. The model for water was SPC-E[5]. The configurations of lowest energy in the classical models reproduce quite well the structures of the DFT minima (figs. 5–2 and table 1).

Simulations in water were performed in the isothermal-isobaric ensemble (NPT) with the Hoover thermo- and barostats, with a timestep of 0.5 fs, the reaction field model of electrostatics ($\epsilon = 78$) and a non-bonded cutoff 12 Å (15 Å in the CTV cluster calculations). We used the molecular dynamics engine DL_CLASSIC, version 1.9[6]. Data analysis was performed with our own routines and Gnuplot[7]. Molecular rendering was done with Avogadro[8] or VMD[9].

3. Photophysical properties of 1a, 1b

Photophsyical properties of **1a**,**1b** are summarised in table 2, page 12

4. Additional information on the ACh-1b complex

The projection procedure used to identify the complex of **1b** with ACh is described in figures 7–8, pp. 13–14. Fig. 9, p. 15 shows the flattening of the *pi* systems of the arms of **1b** due to interaction with ACh.

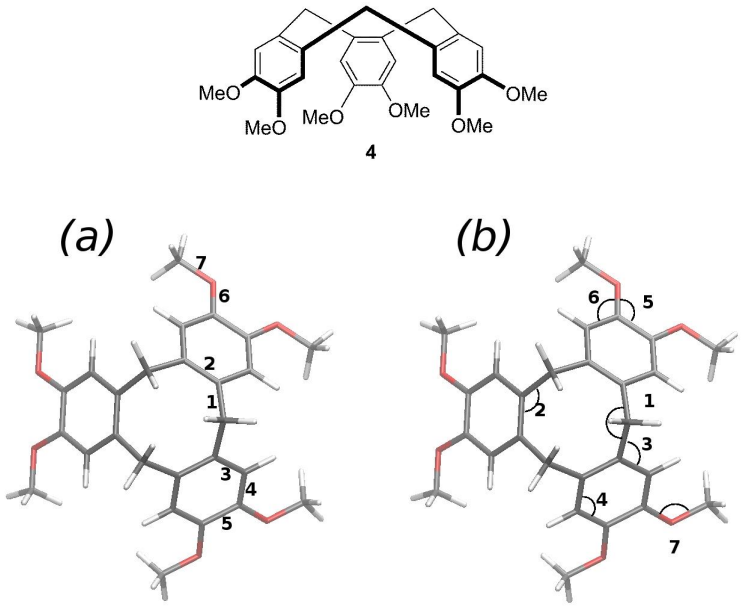

Figure 5: **TOP**: Structure of CTV **4**. **BOTTOM**: Bond, (a), and angle, (b), numbering of **4** for table 1.

	Crystal XRD[a]	B3LYP/6-311G(d,p)	ωB97XD/6-311G(d,p)	MP2/6-31G	Force field
Bond (Å)					
1	1.522(7)/1.515(7)/1.537(7)	1.524	1.517	1.518	1.522
2	1.382(7)/1.378(7)1.399(6)	1.397	1.395	1.392	1.397
3	1.405(7)/1.398(7)/1.406(7)	1.408	1.404	1.402	1.404
4	1.392(7)/1.375(7)/1.382(7)	1.387	1.381	1.381	1.407
5	1.392(7)/1.395(7)/1.403(6)	1.413	1.410	1.413	1.386
6	1.384(6)/1.368(6)/1.375(6)	1.363	1.355	1.357	1.374
7	1.429(7)/1.421(7)/1.430(7)	1.418	1.409	1.415	1.410
Angle (°)					
1	108.5(4)/116.4(5)	114.7	113.2	113.1	113.7
2	124.2(5)/123.8(5)	123.7	123.8	123.6	124.0
3	118.1(4)/117.3(5)	117.6	117.5	117.4	116.8
4	121.2(5)/121.5(5)	122.5	122.4	122.3	121.5
5	124.1(5)/124.1(4)	116.0	116.1	115.9	113.5
6	124.9(4)/124.1(4)	125.2	125.1	125.4	127.1
7	117.7(4)/118.0(5)	118.4	117.9	118.3	118.6

[a]Data from Zhang, H.; Atwood, J. L., J. Cryst. Spectr. Research 1990, 20, 465-470.

Table 1: Bond lengths and angles of CTV **4**, used as a reference in the choice of theoretical methods. See figure 5 for numbering.

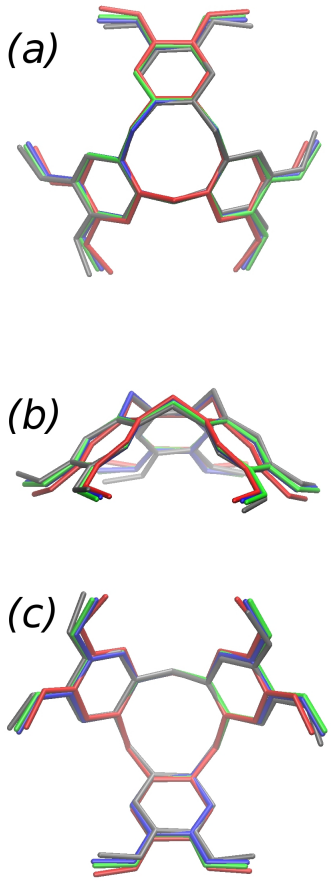

(see footnote, table 1), with the pseudo-mirror plane vertical; in grey, the same molecule rotated 120 ° before alignment, to show up deviations from C_{3v} symmetry imposed by the crystal packing; in blue and green: ωB97XD/6-311G(d,p) and force field (FF) energy minimisations. The root mean squared displacements with respect to the ωB97XD/6-311G(d,p) calculation are 0.09 Å for the FF model and 0.28 Å for both experimental structures (and 0.49 Å between them).

Figure 6: Comparison of the aligned (minimum squared displacement) molecules of CTV **4**. Hydrogens not shown for clarity and not used in the alignment. Top, *(a)*, side, *(b)* and bottom, *(c)*, orthographic views show in red: the structure from the XRD data of Zhang and Atwood

(see footnote, table 1), with the pseudo-mirror plane vertical; in grey, the same molecule rotated 120 ° before alignment, to show up deviations from C_{3v} symmetry imposed by the crystal packing; in blue and green: ωB97XD/6-311G(d,p) and force field (FF) energy minimisations. The root mean squared displacements with respect to the ωB97XD/6-311G(d,p) calculation are 0.09 Å for the FF model and 0.28 Å for both experimental structures (and 0.49 Å between them).

Solute/solvent	λ_{abs}^{max} (nm)	ϵ^{max} ($10^4\,M^{-1}\,cm^{-1}$)	λ_{em}^{max} (nm)	$\delta\lambda_{Stokes}$ (nm)	Φ_F (%)	τ_F (ns)	$\delta\lambda_{abs}^{exp}$ (nm)	$\delta\lambda_{abs}^{th}$ (nm)	O.S.
1a/tetrahydrofuran	302	5.6	390	56	60	1.3	-	-	0.14
	334	5.8				-	-		1.03
1a/acetone	334	5.6	409	75	41	1.8	0	0	1.05
1a/dimethylsulphoxide	338	5.5	422	84	35	3.1	4	2	1.00
1b/PBS buffer, pH 7.4	299	5.6	429	102	21	2.5 (62 %)	-3	-1	0.15
	327	4.9				9 (38 %)	-7	-2	0.97

Table 2: Photophysical properties of CTV **1a**/**1b** in various solvents: λ_{abs}^{max}, λ_{em}^{max}, wavelengths of absorption and emission maxima; ϵ_{max}, maximum molar absorption coefficient; $\delta\lambda_{Stokes}$, Stokes shift; Φ_F, fluorescence quantum yield; τ_F, fluorescence lifetime; λ_{abs}^{exp}, $\delta\lambda_{abs}^{th}$, experimental and theoretical solvation shifts with respect to tetrahydrofuran; O.S., predicted oscillator strength of the first transition. B3LYP/6-31G level of theory.

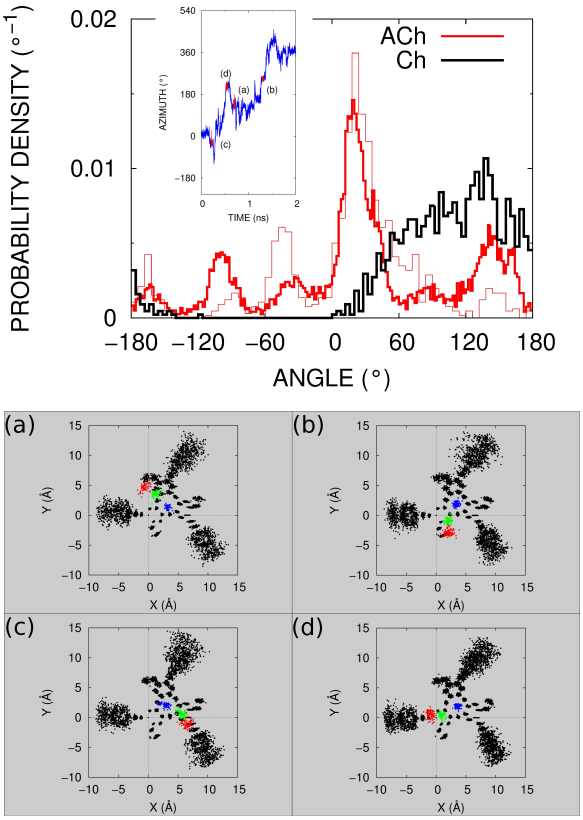

Figure 7: Orthographic projection of complexes between **1b** and ACh or Ch, viewed from below the bowl. The three equivalent **1b** carbon atoms '1' (fig. 1, main text), are brought to a standard positions, one at the origin, one on the Ox axis and one in the Oxy plane. **TOP**: The thick red line shows the distribution of the azimuth (angle in the Oxy plane) of the N—carbonyl O vector of ACh from a 3 ns trajectory (black line, resp. N—hydroxyl O for Ch sampled up to dissociation of the complex at 0.5 ns). The thin red line is for ACh over the same length of sampling period as for Ch. Peak height differences arise slow relaxation compared to the sampling interval achieved here. *Inset:* identifies in red observation periods sampled at 0.5 ps in the botton panel. **BOTTOM**: Scatter diagrams from MD snapshots show the projections of the ACh nitrogen atom (blue), ester oxygen (green) and carbonyl oxygen (red), over the periods referenced in the inset of the top panel. CTV atoms shown in black, except H, omitted for clarity. *(a),(b)*: two of the equivalent main sites; *(c),(d)*: two of the secondary sites.

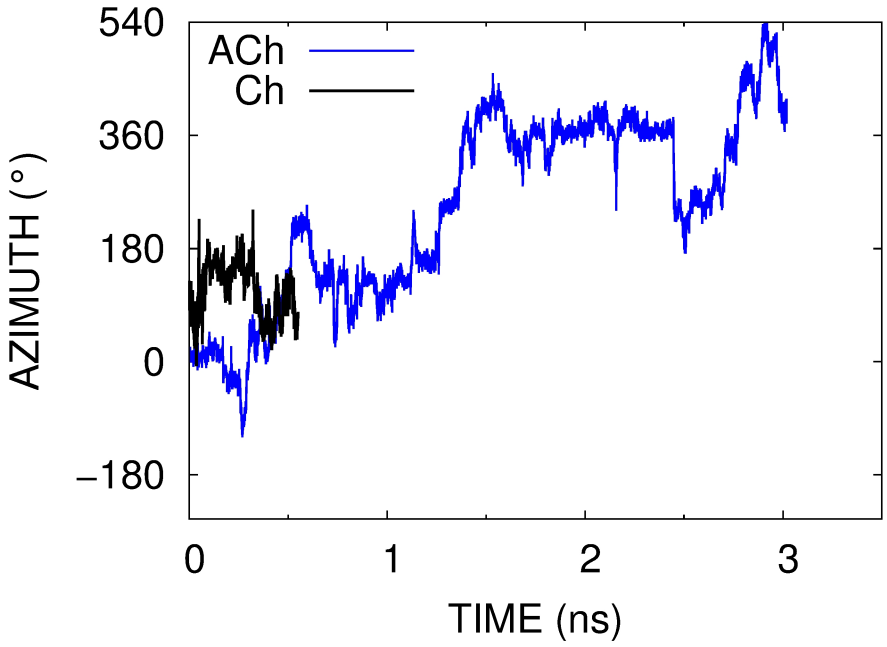

Figure 8: Jumps of the azimuth (see figure SM 7) of the ACh N–carbonyl O direction (coordinate system, see legend figure 7) show ACh (blue line) switching between symmetry-related equivalent sites in the bowl of CTV **1b**. Black line: same for the azimuth of the Ch N–O direction up to the time of dissociation.

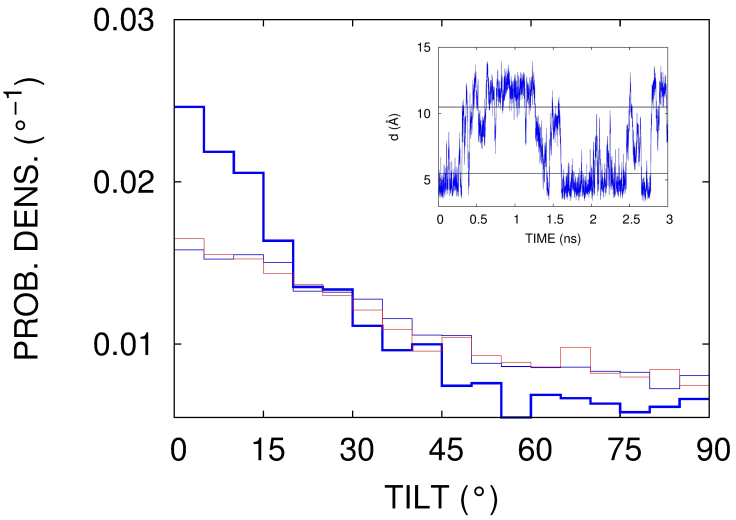

Figure 9: Interaction of ACh with an arm of the CTV flattens the π system. Distribution of the tilt between the planes of the terminal and root phenyl rings on the arms of **1b** free in water (red line) or complexing ACh (blue lines). Thick line: tilts when the ACh terminal methyl group—CTV terminal ring distance d (carbon adjacent to 3 in figure 1), is less than 5.5 Å. Thin lines: $d > 10.5$ Å in the complex (blue) or distribution for free CTV (red). Inset: Sample trajectory of d for one of the arms of the CTV; horizontal lines show the criteria for the histogrammes.

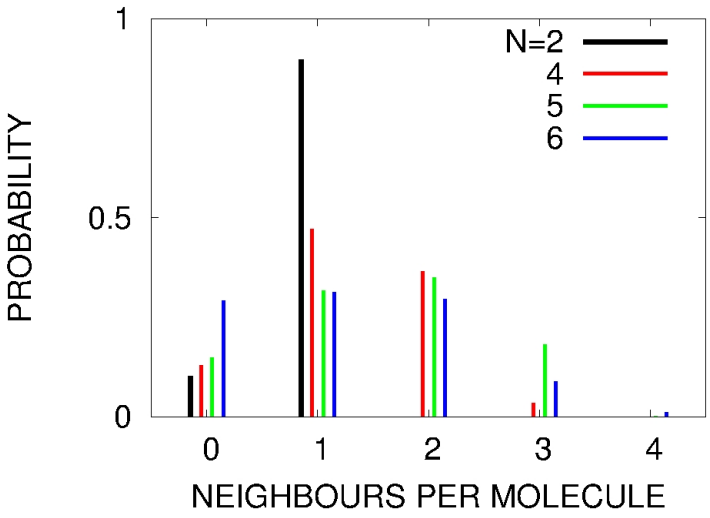

Figure 10: Number of neighbours with $\pi - \pi$ contacts (ring centres less than 4.5 Å apart), per molecule, in clusters of $N = 2$–6 CTV's in water. Data from 2.5 ns MD trajectories.

5. Structure of the CTV clusters

π contacts in the clusters

See figs. 10 and 11 (pp. 16,18) for information on the structure of the clusters. Figure 12, p. 19, shows how the cluster structure depletes water in the region of the π system.

Self-assembly and water depletion

Radial pair correlation functions, $g(r)$, are a simple tool to characterize the average environment at a distance r from a particular atom[10]. Figure 12, p. 19 shows for the $N = 6$ CTV cluster the $g(r)$ between the triple bond carbons (2 or 3 in fig. 1) and the oxygen atom of water. The first solvation shell is visible, up to radius $r = 4.4$ Å. The three arms of the isolated CTV are equivalent, but because of the slow internal dynamics of the clusters (see above), the $g(r)$'s from different arms in the 6 CTV cluster show considerable spread, despite averaging over 2.5 ns of MD trajectory. The (variable) drop of $g(r)$ compared

to the single CTV indicates significant, and heterogeneous depletion of water in the neighbourhood of the C≡C unit.

For example, considering the free **1b** molecule in water, there are on average $\sim$ 5.5 and $\sim$ 5.9 water molecules in the first solvation shell of the inner and outer carbons of the triple bond on each arm, carbons 2 and 3 in figure 1 of the main text. The figures for the 6 CTV cluster range from 2.3 to 5.6 for the internal carbon and from 2.1 to 5.9 for the outer one, with the larger figures corresponding to free arms point into water, and the smaller ones to pairs of strongly $\pi - \pi$ associated arms from adjacent molecules.

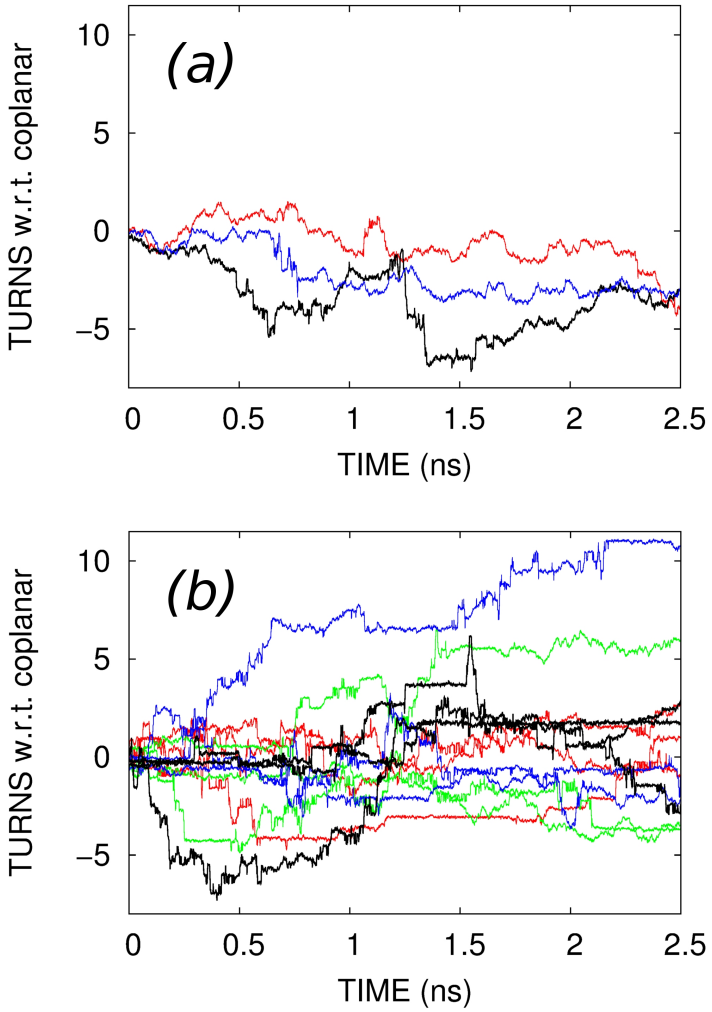

Figure 11: Locking of the terminal rings of the arms of **1b** by π–π contacts in clusters. Trajectories of the dihedral angle between the planes of the arm-rings and their corresponding bowl-ring: *(a)* No locking for a a single CTV in water, three rings coloured by arm; *(b)* Locking in the cluster of 4 CTV's, 12 rings coloured by molecule. Horizontal portions of the trajectories show locking.

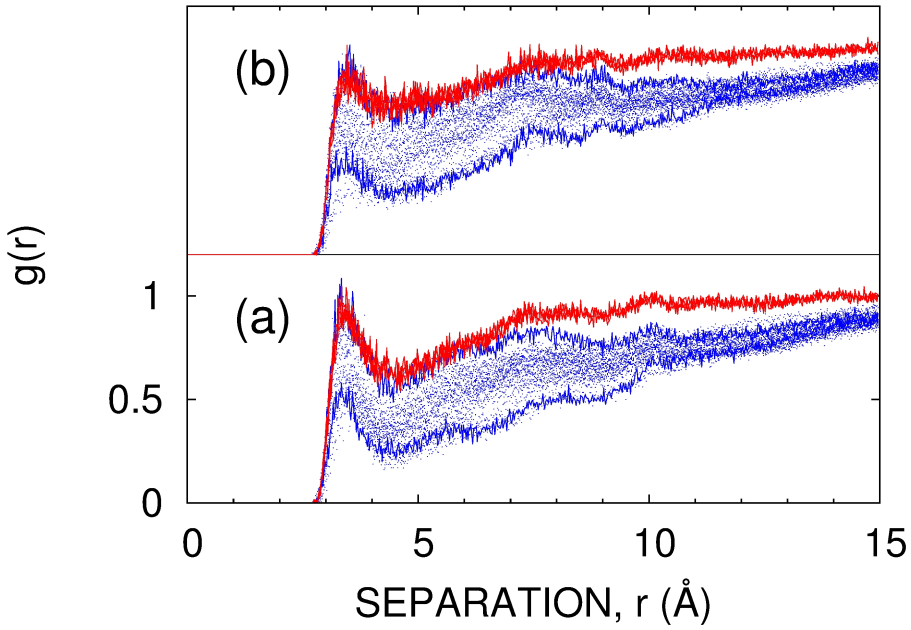

Figure 12: Clustering of the ACh probe **1b** into nanoparticles in water may contribute to the high fluorescence quantum yield by reducing contact between the π system and water. Radial pair correlation functions, $g(r)$,are a simple tool to characterize the average environment at a distance r from a particular atom[10]. The figure shows for the $N = 6$ CTV cluster the $g(r)$ between the triple bond carbons (2 or 3 in fig. 1, main text) and the oxygen atom of water. The first solvation shell is visible, up to radius $r = 4.4$ Å . The three arms of the isolated CTV are equivalent, but because of the slow internal dynamics of the clusters (see ma in text), the $g(r)$'s for different arms in the 6 CTV cluster show considerable spread, despite averaging over 2.5 ns of MD trajectory. *(a)* Inner carbon, 2 in fig. 1; *(b)* outer carbon, 3. Data are shown for the three arms of a single CTV in water (three red lines in each panel) and for the 18 arms of all the molecules in the cluster of 6 CTV's (blue dots). Blue lines: extreme range of pair correlations for particular arms of the cluster.

References

[1] W. H. Melhuish, Quantum efficiencies of fluorescence of organic substances: Effect of solvent and concentration of the fluorescent solute1, J. Phys. Chem. 65 (2) (1961) 229–235. arXiv:http://pubs.acs.org/doi/pdf/10.1021/j100820a009, doi:10.1021/j100820a009.
URL http://pubs.acs.org/doi/abs/10.1021/j100820a009

[2] T. Brotin, J.-P. Dutasta, V. Roy, J. Org. Chem. 70 (2005) 6187–6195.

[3] H. Zhang, J. L. Atwood, Crystal and molecular structure of cyclotriveratrylene, J. Cryst. Spectr. Research 20 (5) (1990) 465–470.

[4] W. L. Jorgensen, D. S. Maxwell, J. Tirado-Rives, Development and testing of the opls all-atom force field on conformational energetics and properties of organic liquids, J. Am. Chem. Soc. 118 (45) (1996) 11225–11236. arXiv:http://pubs.acs.org/doi/pdf/10.1021/ja9621760, doi:10.1021/ja9621760.
URL http://pubs.acs.org/doi/abs/10.1021/ja9621760

[5] H. J. C. Berendsen, J. R. Grigera, T. P. Straatsma, The missing term in effective pair potentials, J. Phys. Chem. 91 (24) (1987) 6269–6271. arXiv:http://pubs.acs.org/doi/pdf/10.1021/j100308a038, doi:10.1021/j100308a038.
URL http://pubs.acs.org/doi/abs/10.1021/j100308a038

[6] W. Smith, T. Forester, I.T.Todorov, The DL_POLY Classic User Manual, version 1.9, STFC Daresbury Laboratory (2012).

[7] T. Williams, C. Kelley, Gnuplot 4.6: an interactive plotting program, URL http://gnuplot.sourceforge.net/ (2014).

[8] M. D. Hanwell, D. E. Curtis, D. C. Lonie, T. Vandermeersch, E. Zurek, G. R. Hutchison, Avogadro: An advanced semantic chemical editor, visualization, and analysis platform, J. Cheminformatics 4 (2014) 17.

[9] W. Humphrey, A. Dalke, K. Schulten, VMD – Visual Molecular Dynamics, J. Mol. Graphics 14 (1996) 33–38.

[10] M. P. Allen, D. J. Tildesley, Computer Simulation of Liquids, OUP, Oxford, UK, 1990.